# Porous scaffold design for tissue engineering

A paradigm shift is taking place in medicine from using synthetic implants and tissue grafts to a tissue engineering approach that uses degradable porous material scaffolds integrated with biological cells or molecules to regenerate tissues. This new paradigm requires scaffolds that balance temporary mechanical function with mass transport to aid biological delivery and tissue regeneration. Little is known quantitatively about this balance as early scaffolds were not fabricated with precise porous architecture. Recent advances in both computational topology design (CTD) and solid free-form fabrication (SFF) have made it possible to create scaffolds with controlled architecture. This paper reviews the integration of CTD with SFF to build designer tissue-engineering scaffolds. It also details the mechanical properties and tissue regeneration achieved using designer scaffolds. Finally, future directions are suggested for using designer scaffolds with *in vivo* experimentation to optimize tissue-engineering treatments, and coupling designer scaffolds with cell printing to create designer material/biofactor hybrids.

## SCOTT J. HOLLISTER

is at the Scaffold Tissue Engineering Group, Departments of Biomedical Engineering, Surgery and Mechnical Engineering, 1107 Gerstacker Building, 2200 Bonisteel Boulevard, The University of Michigan, Ann Arbor, Michigan 41809, USA
e-mail:scottho@umich.edu

Tissue/organ repair has been the ultimate goal of surgery from ancient times to the present. Repair has traditionally taken two forms: (i) tissue grafting and organ transplantation, and (ii) alloplastic or synthetic material replacement. Reconstruction using gold in cranial defects dates back to 2000 BC, and tissue grafting has been used since at least the 1660s[1]. Both approaches, however, have limitations. Grafting requires second surgical sites with associated morbidity and is restricted by limited amounts of material, especially for organ replacement. Synthetic materials often integrate poorly with host tissue and fail over time due to wear and fatigue or adverse body response.

Tissue engineering emerged in the early 1990s to address limitations of tissue grafting and alloplastic tissue repair[2]. The concept is to transplant a biofactor (cells, genes and/or proteins) within a porous degradable material known as a scaffold. The biofactors, which include stem-cell and gene-therapy approaches[3–6], are used to stimulate tissue repair. Far from being a passive component, scaffold material and porous architecture design (here architecture refers to features 10 to 1,000 micrometres in size) play a significant role in tissue regeneration by preserving tissue volume, providing temporary mechanical function, and delivering biofactors. A successful scaffold should balance mechanical function with

biofactor delivery, providing a sequential transition in which the regenerated tissue assumes function as the scaffold degrades. This balance often presents a tradeoff between a denser scaffold providing better function and a more porous scaffold providing better biofactor delivery. The architect Robert le Ricolais stated "The art of structure is where to put the holes". For tissue engineering a suitable paraphrase would be "The art of scaffolding is where to put the holes and the biofactors". This paper reviews how integration of computational topology design (CTD) and solid free-form fabrication (SFF) have made scaffolds with designed characteristics possible, and how these design characteristics have affected scaffold mechanical and biological performance.

## COMBINING MECHANICAL FUNCTION AND TISSUE REGENERATION

Approaches in scaffold design must be able to create hierarchical porous structures to attain desired mechanical function and mass transport (that is, permeability and diffusion) properties, and to produce these structures within arbitrary and complex three-dimensional (3D) anatomical shapes. Hierarchical refers to the fact that features at scales from the nanometre to millimetre level will determine how well the scaffold meets conflicting mechanical function and mass-transport needs. Material chemistry together with processing determines the maximum functional properties that a scaffold can achieve, as well as how cells interact with the scaffold. However, mass-transport requirements for cell nutrition, porous channels for cell migration, and surface features for cell attachment necessitate a porous scaffold structure. This porous

structure dictates that achievable scaffold properties will fall between the theoretical maximum set by the material and the theoretical minimum of zero predicted by composite theories[7,8]. The critical issue for design is then to compute the precise value of mechanical as well as mass-transport properties at a given scale based on more microscopic properties and structure.

One way to achieve hierarchical design is to create libraries of unit cells (a mathematical entity not to be confused with a biological cell) at different physical scales that can be assembled to form scaffold architectures. Such libraries may be created either using image-based design approaches[9–11], or using approaches based on computer-aided design (CAD)[12–17]. Homogenization theory, which uses asymptotic expansion of relevant physical variables to generate multiscale equilibrium equations[18–20] can then be used to compute effective properties based on these unit-cell designs. By solving unit-cell deformation under six local strain states, the effective stiffness at a more macroscopic level $C_{ijkl}^{\text{macro}}$ is computed from the stiffness at a more microscopic level $C_{ijpm}^{\text{micro}}$, and the 3D spatial arrangement of the microscopic level as given by the strain localization tensor $M_{pmkl}$ and the volume of the unit cell ($V_{\text{unit cell}}$):

$$C_{ijkl}^{\text{macro}} = \frac{1}{\left|V_{\text{unit cell}}\right|} \int_V C_{ijpm}^{\text{micro}} \; M_{pmkl} \; dV_{\text{unit cell}} \quad (1)$$

Note that homogenization analysis for elastic properties may be applied recursively across hierarchical scales to compute how the smallest features through to the largest features contribute to overall scaffold elastic properties.

For mass-transport purposes, the macroscopic permeability $K_{ij}^{\text{macro}}$ is computed based on the average Stokes' flow velocity $v_j^i$ vectors calculated in response to three separately applied unit pressure gradients:

$$K_{ij}^{\text{macro}} = \frac{1}{\left|V_{\text{unit cell}}\right|} \int_V v_j^i \; dV_{\text{unit cell}} \quad (2)$$

As expected, increasing the amount of material increases elastic properties while decreasing permeability for a particular scaffold design (Fig. 1). However, for a given porosity, different scaffold microstructures will lead to different effective stiffness and permeability. This analysis further demonstrates that material/pore arrangement ("putting the holes") determines what mechanical properties may be achieved within the bound set by material chemistry. Furthermore, effective permeability is only determined by the 3D pore arrangement.

Going beyond effective property computation from defined microstructures, topology optimization approaches[11,21,22] actually compute new microstructures to attain desired properties. These approaches have either been used to optimize functional elastic properties with a constraint on porosity, or to maximize permeability with a constraint on desired elastic properties and permeability. We have used this technique to design microstructures whose permeability is maximized for cell migration and mass
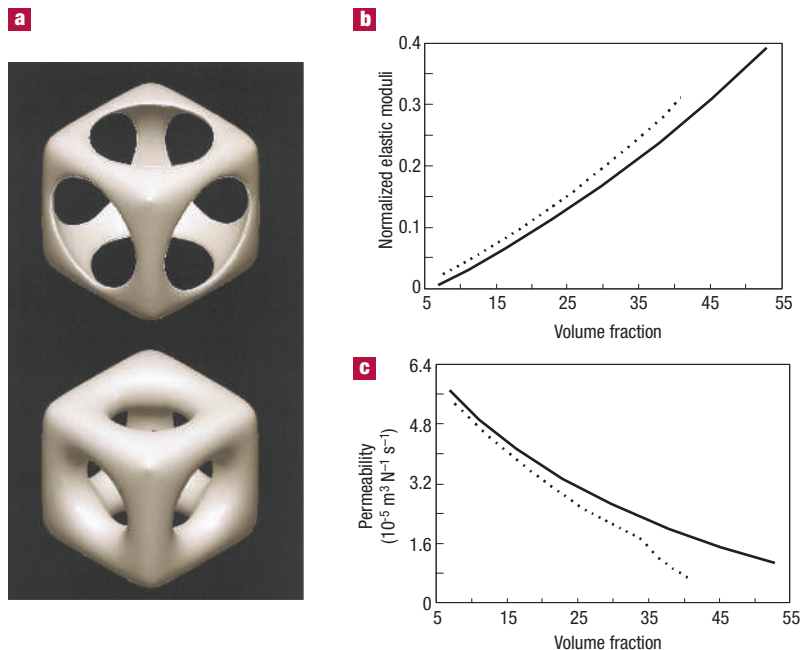
transport, but whose effective linear elastic properties match those of natural bone tissue (Fig. 2).

The final stage of design is to create the scaffold architecture within any arbitrarily complex 3D anatomic defect. This stage draws heavily on commonly used medical imaging modalities, especially computed tomography (CT) and magnetic resonance imaging (MRI), and directly introduces patient medical information into the scaffold fabrication process. Both CT and MRI produce structured voxel datasets where patient anatomy is defined by density distribution. The anatomic defect shape of interest is isolated from the CT or MRI scan. At this point, the global anatomic defect of interest is represented as density data within a voxel data subset. This data must be used in the design process. The two primary methods for achieving this are either by converting the voxel anatomic data into solid geometric models for use in CAD[12–16], or by directly using voxel database structures in image-based methods[9,10]. The defined anatomic defected shape is then intersected with the microstructure design database using boolean techniques, resulting in the final scaffold design. Hierarchical scaffolds with desired anatomic shape and known functional and mass-transport properties can be designed by integrating global anatomic image data with either predefined or optimized unit-cell architectures. Figure 3 demonstrates the image-based design technique integrated with fabrication to produce a final scaffold.

## FABRICATION AND PERFORMANCE OF DESIGNED SCAFFOLDS

Determining how or even if designer scaffolds can improve tissue-engineering treatment requires that these scaffolds can be first fabricated and then tested for mechanical function and tissue regeneration. Fabrication is a significant hurdle. Complex scaffold architecture designs

**Figure 1** Modulus versus porosity and permeability versus porosity for two designed spherical pore and cylindrical pore microstructures. **a**, Example of the spherical pore (top) and cylindrical pore (bottom) microstructures. **b**, Plot of effective elastic moduli normalized by base moduli for spherical pore (dashed line) and cylindrical pore (solid line). Results demonstrate that the modulus increases as expected with volume fraction, and that for a given volume fraction the spherical pore is stiffer. **c**, Plot of effective permeability for spherical pore (dashed line) and cylindrical pore (solid line). Results demonstrate that permeability decreases as expected with volume fraction and that for a given volume fraction the cylindrical pore design is more permeable.

**a**
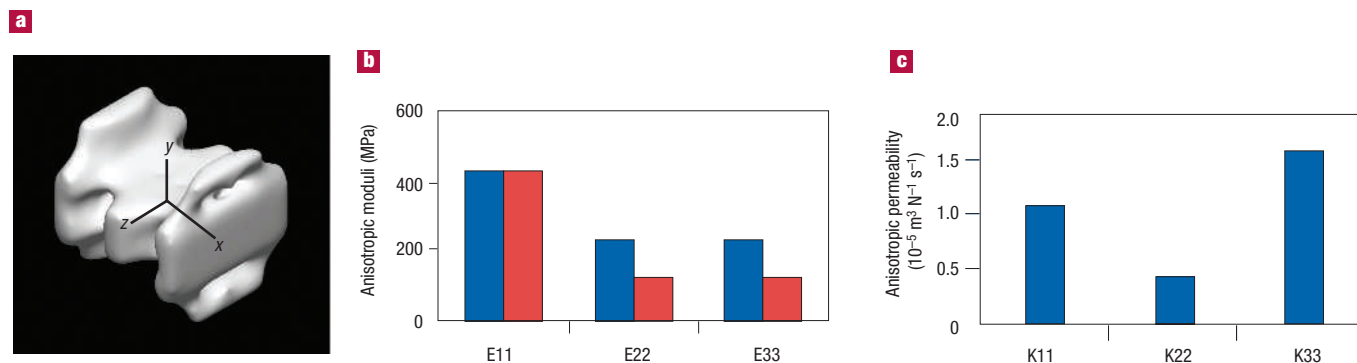


**Figure 2** Example of designed microstructure optimized for maximum permeability with a constraint that effective modulus matches human mandibular condyle bone tissue and a porosity constraint of 54%. **a**, Designed unit-cell microstructure. **b**, Comparison of effective anisotropic moduli for natural bone and designed microstructure. Blue denotes design moduli and red denotes target moduli. **c**, Resulting anisotropic permeability of designed microstructure. Work of Cheng Yu Lin with the author.
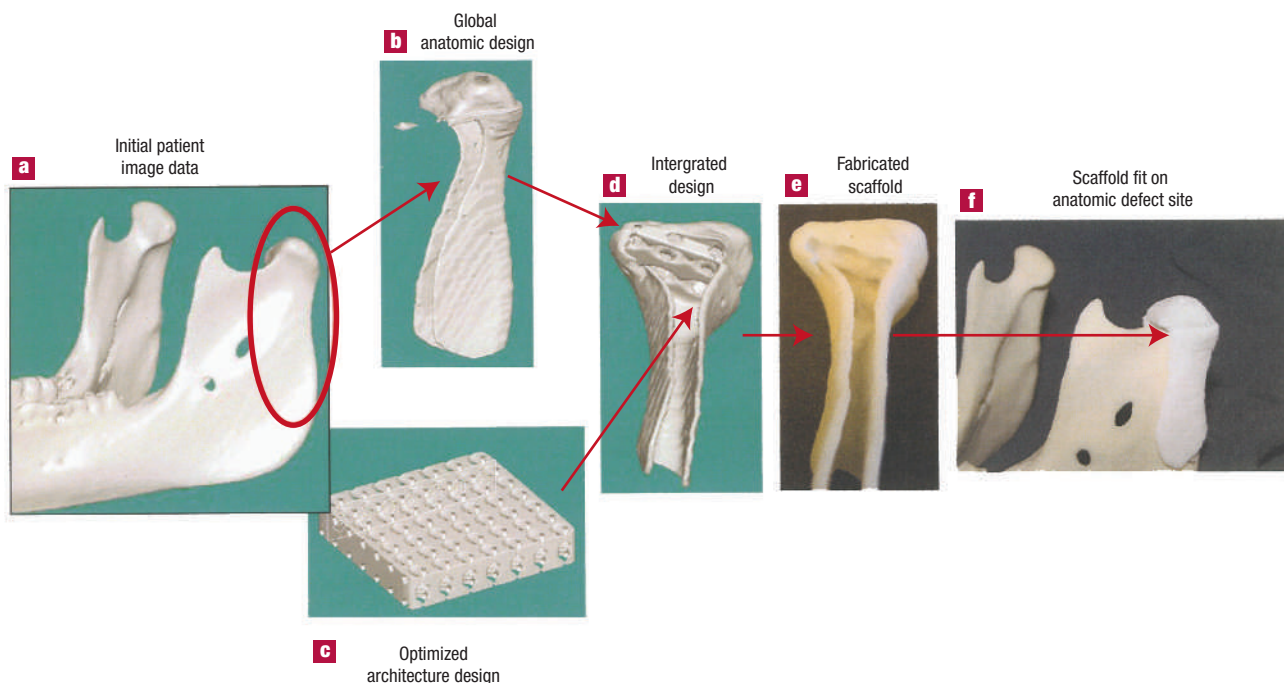


**Figure 3** Image-based procedure for integrating designed microstructure with anatomic shape. **a**, A CT (as shown here) or MRI scan serves as starting point for designing scaffold exterior. **b**, The scaffold exterior shape is created with additional features for surgical fixation. **c**, Architecture image-design is created using CTD. **d**, Global anatomic and architecture design are integrated using boolean image techniques. **e**, SFF is used to fabricate design from degradable biomaterial, in this case SLS was used to fabricate a PCL scaffold (fabricated scaffold created by Suman Das). **f**, Final fabricated scaffold fits well on the intended anatomic reconstruction site.
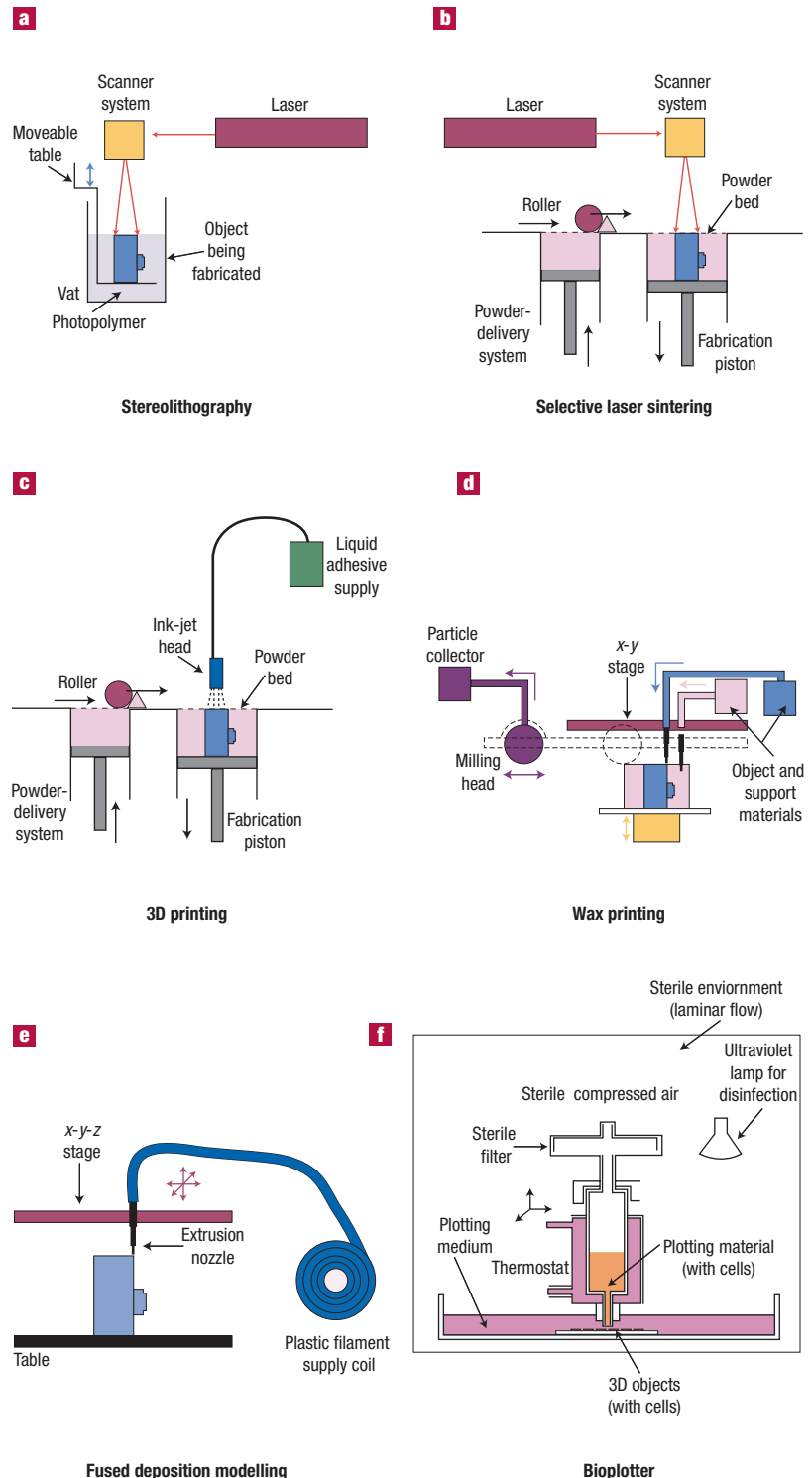
generated using hierarchical image-based or CAD techniques cannot readily be built using conventional techniques. Instead, scaffold architectures must be built using layer-by-layer manufacturing processes known collectively as SFF. A number of articles have reviewed and compared SFF scaffold fabrication methods[23–27], so this section will only briefly review SFF techniques, instead concentrating on how designer scaffolds have performed, and future directions for their use in tissue-engineering therapies.

All SFF systems use a triangular facet surface representation of a structure, and build the 3D structure on a platform that moves to allow layering. Commercially available systems may be categorized into three major groups based on the way materials are deposited (Fig. 4). The first group includes laser-based machines that either photopolymerize liquid monomer (Fig. 4a) or sinter powdered materials (Fig. 4b). The second major group actually prints material, including printing a chemical binder onto powdered material (Fig. 4c) or directly printing wax (Fig. 4d). The third

major group is of nozzle-based systems, which process material either thermally or chemically as it passes through a nozzle (Fig. 4e,f). This class of systems include the Bioplotter, which is the only commercial machine developed to print biological cells as well as a range of biomaterials. Numerous studies have used both commercial and custom-built systems for scaffold fabrication using both direct and indirect methods[28–46], including combining SFF with traditional scaffold-processing techniques to fabricate hierarchical scaffolds with micrometre to millimetre features[47–49]. As fabrication feasibility has been amply demonstrated, the critical issue becomes how designer scaffolds perform with regard to traditional scaffolds.
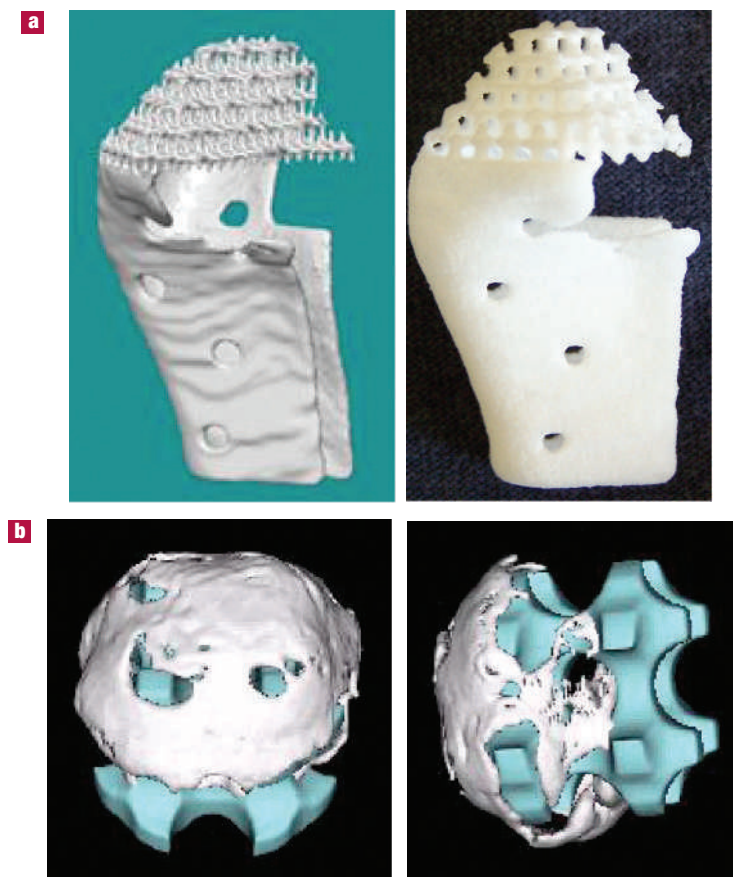
Providing adequate mechanical support is a critical scaffold requirement. If the scaffold cannot provide a mechanical modulus in the range of hard (10–1,500 MPa)[50] or soft tissues (0.4–350 MPa)[51], then any nascent tissue formation will probably also fail due to excessive deformation. Scaffolds made using traditional polymer-processing techniques, such as porogen leaching[52,53] or gas foaming[52], have maximum compressive moduli of 0.4 MPa, well below hard tissue or most soft tissues. Designed scaffold architecture has clearly made improvements in scaffold mechanical performance. Three-dimensional printing (3DP) has been used[54] to fabricate discrete phase composite scaffolds from D,L-polylactic-polyglycolic acid (PLGA)/L-polylactic acid (L-PLA) in one phase and a L-PLGA/tri-calcium phosphate mixture in the second phase. Peak polymer/ceramic phase elastic modulus and yield strength were 450 MPa and 13.7 MPa, respectively. A fused deposition modelling nozzle technique was developed[55] for polycaprolactone (PCL) that produced scaffolds with porosity ranging from 48% to 77%, and compressive moduli and yield strength ranged from 4 to 77 MPa and 2.58 to 3.32 MPa, respectively. A laser technique, selective laser sintering (SLS), was used[56] to fabricate PCL scaffolds that had porosity ranging from 37–55%, compressive moduli ranging from 52 to 68 MPa, and strength ranging from 2.0 to 3.2 MPa. The measured mechanical modulus correlated well with image-based finite-element predictions, demonstrating that scaffold mechanical modulus could be predicted by image-based design. PCL scaffolds were also fabricated to match mandibular condyle anatomic designs (Fig. 5). In addition to direct scaffold fabrication, SFF has been used to fabricate scaffold moulds for casting biomaterials. Hydroxyapatite (HA) has been cast[57] into printed wax moulds, creating scaffolds with pores between 366 and 444 μm having compressive modulus and strength of 1,400 ± 400 MPa and 30 ± 8 MPa, respectively.

For soft-tissue applications, a group of researchers from the University of Twente and IsoTis engineered scaffolds by depositing poly(ethylene glycol)-terephthalate (PEG/PBT) fibres with the Bioplotter[58–60]. The scaffolds had orthogonal pore structures ranging in size from 185 to 1,683 μm. Scaffold static and dynamic moduli were 0.05–2.5 MPa and 0.16–4.33 MPa, respectively, within the range of native cartilage values (0.27 static, 4.10 dynamic). Saito et al.[61] created a wavy fibre scaffold architecture design with varying fibre pitch angles fabricated from PCL using SLS. They demonstrated compressive moduli ranging from 4

**Stereolithography**

**Selective laser sintering**

**3D printing**

**Wax printing**

**Fused deposition modelling**

**Bioplotter**

**Figure 4** Schematics of SFF systems categorized by the processing technique. **a,b**, Laser-based processing systems include the stereolithography system, which photopolyermerizes a liquid (**a**) and the SLS systems, which sinter powdered material (**b**). In each system, material is swept over a build platform that is lowered for each layer. **c,d**, Printing-based systems, including 3D printing (**c**) and a wax printing machine (**d**). 3DP prints a chemical binder onto a powder bed. The wax-based system prints two types of wax material in sequence. **e,f**, Nozzle-based systems. The fused deposition modeller prints a thin filament of material that is heated through a nozzle (**e**). The Bioplotter prints material that is processed either thermally or chemically (**f**). The Worldwide Guide to Rapid Prototyping (C) Copyright Castle Island Co. All rights reserved. http://home.att.net/~castleisland/.

**Figure 5** Examples of PCL scaffolds directly fabricated using SLS. **a**, Mandibular condyle design and PCL scaffold fabricated by SLS. **b**, Two views of bone growth into PCL scaffold. White is bone image and blue is scaffold image. Work from Suman Das, Paul Krebsbach, Jessica Williams, Rachel Schek, Brock Partee, Colleen Flanagan and the author.

suggested. However, unlike the single pore diameter in the designed scaffolds, non-designed scaffolds have a range of pore sizes, which may explain the different results. Optimally designed PPF/TCP scaffolds with a modulus of 140 MPa have been used to deliver BMP-7 transduced human gingival fibroblasts in a mouse model[67]. Empty scaffolds degraded to a modulus of 38 MPa after eight weeks but scaffolds delivering transduced cells had a modulus of 65 MPa at eight weeks after bone regeneration. Malda *et al.*[60] compared cartilage regeneration for designer orthogonal pore scaffolds and those made by porogen leaching, both seated with chondrocytes. They found that the designed scaffolds exhibited significantly higher glycosaminoglycan content, a significant component in articular cartilage matrix. Their results demonstrated significantly higher oxygen diffusion and cartilage matrix regeneration in the designed scaffolds. This difference could be attributed to many factors, including better cell seeding in the scaffold interior, lower oxygen gradients, and better cell aggregation in the designed scaffolds[59]. Finally, using image-designed and SFF polymer/ ceramic composites, a multiple tissue interface of bone and cartilage was engineered by seeding BMP-7 transduced cells on the ceramic portion and porcine chondrocytes on the polymer portion[68]. This demonstrated the capability of interfacing designed scaffolds to create tissue interfaces.

To date, biofactors have been seeded or positioned into designed scaffolds using techniques, which although effective, offer virtually no control over exact 3D positioning of or the use of multiple biofactors. The ultimate solution is to simultaneously print the biofactors with the scaffold material. Owing to the hostile processing environment required for most materials, cells are printed in hydrogels. Commercially available ink-jet printing heads have been converted to print cells and proteins, and their viability has been demonstrated for printing Chinese hamster ovarian cells[69–71]. The Bioplotter has been used to print viable cells in agar (reported in ref. 72). Chondrocytes were printed within alginate in the shape of knee meniscus[73], and was the first demonstration of cells printed in an anatomic shape. These studies, though very preliminary, demonstrate that printing viable cells is feasible.

## PRESENT AND FUTURE

Hierarchical computational techniques have allowed design of 3D anatomic scaffolds with porous architecture that balances function and mass transport. SFF has allowed fabrication of scaffolds with controlled architecture from polymer, hydrogel, ceramic and even metal biomaterials. These scaffolds have significantly better mechanical properties than scaffolds processed using other methods. These improved mechanical properties are especially important for bone-tissue engineering, which has much greater stiffness and strength than other tissues. However, even for soft tissue, scaffolds made using traditional methods often are not adequate mechanically. The need for adequate scaffold mechanical properties, coupled with a wide range of scaffold base-material properties, necessitates the ability to control scaffold mechanical properties

to 17 MPa tensile moduli 20 to 70 MPa, and ultimate strains ranging from 8% to 35%, all for scaffolds with the same 70% porosity. These moduli and ultimate strain values are within the range of most soft-tissue values. They also demonstrated that selected fibre designs would exhibit nonlinear stress–strain curves similar to soft tissues because of fibre contact.

A number of architectural characteristics including porosity, pore size and permeability play a significant role in biological delivery and tissue regeneration. Here again, the ability to rigorously control scaffold architecture can provide significant insights into how scaffold architecture and material affect tissue regeneration. As a first step, numerous research groups have demonstrated that SFF scaffolds support cell attachment *in vitro*[31,35,37,47,49,54,55] and single tissue regeneration *in vivo*[45,57,58,63,64]. Designer scaffolds are now being used to specifically study architectural influence on tissue regeneration. Two groups[64,65] found no significant difference in bone growth for 500 μm and 1,600 μm pores for PLGA scaffolds made by a 3D printing technique. Our group[66] used designed HA scaffolds with pore diameters ranging between 400 μm and 1,200 μm in a minipig mandibular defect model and HA scaffolds with 300 μm and 800 μm to deliver human gingival fibroblasts transduced with BMP-7 in a mouse model. We found significant bone growth on designed scaffolds for all pores, with no statistical difference between pore sizes. This contrasts results using non-SFF scaffolds, where optimal pore diameters ranging from 200 μm to 600 μm have been

through architecture topology design. Although initial steps have been made in linking CTD and SFF, future work must determine how closely designed scaffolds can attain desired mechanical properties as a function of material and SFF processing method.

Designer scaffolds have achieved higher bone and cartilage regeneration compared with other scaffolds, probably due to high interconnected porosity. The benefits of interconnected porosity include improved cell seeding and channels to guide cell migration and tissue ingrowth. Cell guidance is important not only for bone and cartilage regeneration, but is also believed to be critical for neural regeneration[74]. In addition, the ability to seed multiple cell types on composite scaffolds has opened the door to multiple tissue and tissue-interface regeneration[54,68]. However, despite these initial studies, much remains to be investigated regarding the effect of designed scaffold architecture on tissue regeneration. For example, does increased permeability enhance tissue regeneration? Is there an optimal material for regeneration of specific tissues? How should multiple materials be interfaced to generate tissue interfaces? Answering these and other questions requires *in vivo* experiments using scaffolds made with controlled characteristics. Designer scaffolds would make a significant impact on tissue-engineering treatments solely by addressing these issues, which cannot be resolved using scaffolds not having designed architecture.

Although current design/fabrication occurs at scales above 100 μm, future work should also strive to incorporate micrometre- and nanoscale features. Currently, integration of micrometre or tens of micrometre feature sizes occurs during post-processing steps[47–49]. Integration of micrometre- and nanoscale features into designed scaffolds could improve both mechanical properties through toughening mechanisms and tissue regeneration through improved control of cell adhesion. However, near-term advances in this area will probably occur through post-processing or a combination of nanofabrication techniques with indirect SFF.

The ultimate designer material/biofactor hybrid would have computationally optimized 3D structural and biofactor topology with the material and biofactor fabricated simultaneously. This depends first on elucidating, through experiments with designed scaffolds, how scaffold structure and biofactor affect tissue regeneration. Second, it depends on advancing biofactor printing techniques in conjunction with other SFF material processing technology. Although hydrogel techniques are optimal for biofactor printing, hydrogels do not possess the functional characteristics needed for reconstruction of hard tissue and most soft tissue. Therefore, advances in this area may come from multiple nozzle systems providing separate processing of biofactors and scaffold materials but allow deposition on the same platform. Culmination of such efforts in the coming decades could lead to pre-packaged designer tissue replacements created from patient medical informatics (images and medical history) and printed with 3D distributions of materials, cells, genes and proteins optimized for tissue regeneration.

doi: 10.1038/nmat1421
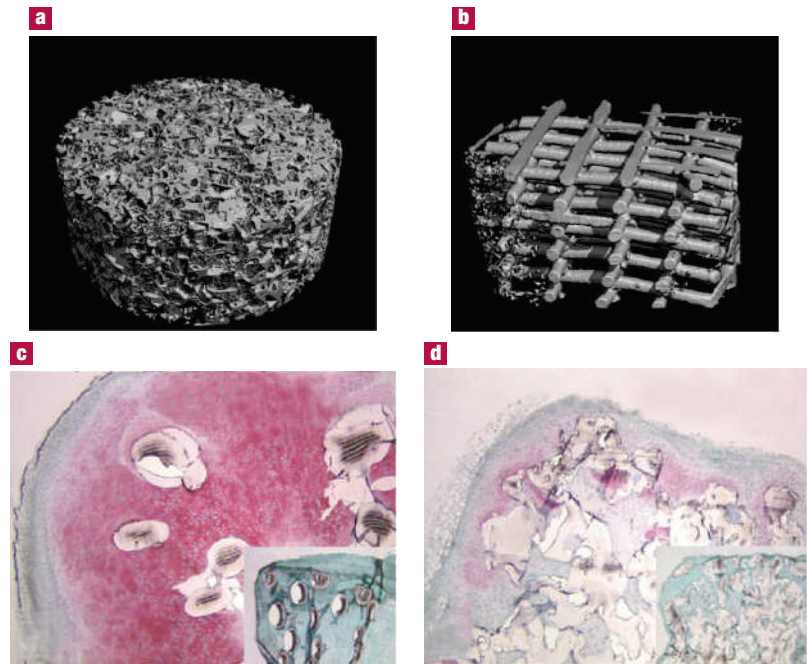
**Figure 6** Cartilage regeneration by chondrocyte delivery on designed Bioplotter-fabricated PEG/PBT scaffolds is superior to PEG/PBT scaffolds made by porogen leaching. **a**, Bioplotter-fabricated PEG/PBT scaffold. **b**, PEG/PBT scaffold fabricated by porogen leaching. **c**, Cartilage matrix (red areas) generation in Bioplotter scaffold after 21 days in a mouse. Insert shows scaffold implanted without chondrocytes. **d**, Cartilage matrix (red area) generation after 21 days in scaffold made by porogen leaching. Insert shows control scaffold implanted without chondrocytes. Reprinted from ref. 61. Copyright (2005), with permission from Elsevier.

## References

1. Sanan, A. & Haines, S. J. Repairing holes in the head: a history of cranioplasty. *J. Neurosurg.* **40,** 588–603 (1997).
2. Langer, R. & Vacanti, J. P. Tissue engineering. *Science* **260,** 920–926 (1993).
3. Audet, J. Stem cell bioengineering for regenerative medicine. *Expert Opin. Biol. Ther.* **4,** 631–644 (2004).
4. Caplan, A. I., Reuben, D. & Haynesworth, S. E. Cell-based tissue engineering therapies: the influence of whole body physiology. *Adv. Drug Deliv. Rev.* **33,** 3–14 (1998).
5. Bonadio, J. Tissue engineering via local gene delivery. *J. Mol. Med.* **78,** 303–311 (2000).
6. Cutroneo, K. R. Gene therapy for tissue regeneration. *J. Cell Biochem.* **88** 418–425 (2003).
7. Hashin, Z. & Shtrikman, S. A variational approach to the theory of the elastic behavior of multiphase materials. *J. Mech. Phys. Solids* **11,** 127–140 (1962).
8. Torquato, S. *Random Heterogenous Materials: Microstructure and Macroscopic Properties* (Springer, New York, 2002).
9. Hollister, S. J., Lev,y R. A., Chu, T. M., Halloran, J. W. & Feinberg, S. E. An image-based approach for designing and manufacturing craniofacial scaffolds. *Int. J. Oral Maxillofac. Surg.* **29,** 67–71 (2002).
10. Hollister, S. J., Maddox, R. D. & Taboas, J. M. Optimal design and fabrication of scaffolds to mimic tissue properties and satisfy biological constraints. *Biomater.* **23,** 4095–4103 (2002).
11. Lin, C. Y., Kikuchi, N. & Hollister, S. J. A novel method for biomaterial scaffold internal architecture design to match bone elastic properties with desired porosity. *J. Biomech.* **37,** 623–636 (2004).
12. Sun, W., Starly, B., Darling, A. & Gomez, C. Computer-aided tissue engineering: application to biomimetic modelling and design of tissue scaffolds. *Biotechnol. Appl. Biochem.* **39,** 49–58 (2004).
13. Sun, W., Darling, A., Starly, B. & Nam, J. Computer-aided tissue engineering: overview, scope and challenges. *Biotechnol. Appl. Biochem.* **39,** 29–47 (2004).
14. Fang, Z., Starly, B. & Sun, W. Computer-aided characterization for effective mechanical properties of porous tissue scaffolds. *Comput. Aid. Design* **37,** 65–72 (2005).
15. Cheah, C. M., Chua, C. K., Leong, K. F., Cheong, C. H. & Naing, M. W. Automatic algorithm for generating complex polyhedral scaffold structures for tissue engineering. *Tissue Eng.* **10** 595–610 (2004).

16. Van Cleynenbreugel, T., Van Oosterwyck, H., Vander Sloten J. & Schrooten J. Trabecular bone scaffolding using a biomimetic approach. *J. Mater Sci. Mater. Med.* **13,** 1245–1249 (2002).

17. Yang, S., Leong, K. F., Du, Z. & Chua, C. K. The design of scaffolds for use in tissue engineering. Part II. Rapid prototyping techniques. *Tissue Eng.* **8,** 1–11 (2002).

18. Sanchez-Palencia, E. & Zaoui, A. *Homogenization Techniques for Composite Media* (Springer, Berlin, 1987).

19. Hollister, S. J. & Kikuchi, N. Homogenization theory and digital imaging: a basis for studying the mechanics and design principles of bone tissue. *Biotech. Bioeng.* **43,** 586–596 (1994).

20. Terada, K., Ito T. & Kikuchi, N. Characterization of the mechanical behaviors of solid-fluid mixture by the homogenization method. *Comp. Meth. App. Mech. Eng.* **153,** 223–257 (1998).

21. Sigmund, O. Materials with prescribed constitutive parameters – an inverse homogenization problem. *J. Solids Struct.* **31,** 2513–2529 (1994).

22. Lin, C. Y., Hsiao, C. C., Chen P. Q. & Hollister, S. J. Interbody fusion cage design using integrated global layout and local microstructure topology optimization. *Spine* **29,** 1747–1754 (2004).

23. Hutmacher, D. W., Sittinger, M. & Risbud, M. V. Scaffold-based tissue engineering: rationale for computer-aided design and solid free-form fabrication systems. *Trends Biotechnol.* **22,** 354–362 (2004).

24. Leong, K. F., Cheah, C. M. & Chua, C. K. Solid freeform fabrication of three-dimensional scaffolds for engineering replacement tissues and organs. *Biomaterials* **24,** 2363–2378 (2003).

25. Sachlos, E. & Czernuszka, J. T. Making scaffolds work: a review on the application of solid freeform fabrication technology to the production of tissue engineering scaffolds. *Eur. Cell Mater.* **5,** 29–40 (2003).

26. Tsang, V. L. & Bhatia, S. N. Three dimensional tissue fabrication. *Adv. Drug Deliv.* **56,** 1635–1647 (2004).

27. Yeong, W. Y., Chua, C. K., Leong, K. F. & Chandrasekaran, M. Rapid prototyping in tissue engineering: challenges and potential. *Trends Biotechnol.* **22,** 643–652 (2004).

28. Bose, S. *et al.* Processing and characterization of porous alumina scaffolds. *J. Mater. Sci. Mater. Med.* **13,** 23–28 (2002).

29. Chu, T. M., Hollister, S. J., Halloran, J. W., Feinberg, S. E. & Orton, D. G. Manufacturing and characterization of 3-d hydroxyapatite bone tissue engineering scaffolds. *Ann. NY Acad. Sci.* **961,** 114–117 (2002).

30. Chua, C. K., Leong, K. F., Tan, K. H., Wiria, F. E. & Cheah, C. M. Development of tissue scaffolds using selective laser sintering of polyvinyl alcohol/hydroxyapatite biocomposite for craniofacial and joint defects. *J. Mater. Sci. Mater. Med.* **15,** 1113–1121 (2004).

31. Ciardelli, G. *et al.* Innovative tissue engineering structures through advanced manufacturing technologies. *J. Mater. Sci. Mater. Med.* **15,** 305–310 (2004).

32. Cooke, M. N., Fisher, J. P., Dean, D., Rimnac, C. & Mikos, A. G. Use of stereolithography to manufacture critical-sized 3D biodegradable scaffolds for bone ingrowth. *J. Biomed. Mater. Res.* **64B,** 65–69 (2003).

33. Dhariwala, B., Hunt, E. & Boland, T. Rapid prototyping of tissue-engineering constructs, using photopolymerizable hydrogels and stereolithography. *Tissue Eng.* **10,** 1316–1322 (2004).

34. Fisher, J. P. *et al.* A. Soft and hard tissue response to photocrosslinked poly(propylene fumarate) scaffolds in a rabbit model. *J. Biomed. Mater. Res.* **59,** 547–556 (2002).

35. Giordano, R. A. *et al.* Mechanical properties of dense polylactic acid structures fabricated by three dimensional printing. *J. Biomater. Sci. Polym. Edn* **8,** 63–75 (1996).

36. Hutmacher, D. W. *et al.* Mechanical properties and cell cultural response of polycaprolactone scaffolds designed and fabricated via fused deposition modeling. *J. Biomed. Mater. Res.* **55,** 203–216 (2001).

37. Khalil, S., Nam J. & Sun, W. Multi-nozzle deposition for construction of 3D biopolymer tissue scaffolds. *Rapid Prototyp. J.* **11,** 9–17 (2005).

38. Landers, R., Hubner, U., Schmelzeisen, R. & Mulhaupt, R. Rapid prototyping of scaffolds derived from thermoreversible hydrogels and tailored for applications in tissue engineering. *Biomaterials* **23,** 4437–4447 (2002).

39. Levy, R. A., Chu, T. M., Halloran, J. W., Feinberg, S. E. & Hollister, S. J. CT-generated porous hydroxyapatite orbital floor prosthesis as a prototype bioimplant. *Am. J. Neuroradiol.* **18,** 1522–1525 (1997).

40. Pfister, A. *et al.* Biofunctional rapid prototyping for tissue-engineering applications: 3D bioplotting versus 3D printing. *J. Polym. Sci.* **42,** 624–638 (2004).

41. Sodian, R. *et al.* Application of stereolithography for scaffold fabrication for tissue engineered heart valves. *Am. Soc. Artificial Internal Organs J.* **48,** 12–16 (2002).

42. Tan, K. H. *et al.* Selective laser sintering of biocompatible polymers for applications in tissue engineering. *Biomed. Mater. Eng.* **15,** 113–124 (2005).

43. Vozzi, G., Flaim, C., Ahluwalia, A. & Bhatia, S. Fabrication of PLGA scaffolds using soft lithography and microsyringe deposition. *Biomaterials* **24,** 2533–2540 (2003).

44. Wang, F. *et al.* Precision extruding deposition and characterization of poly-e-caprolactone tissue scaffolds. *Rapid Prototype J.* **10,** 42–49 (2004).

45. Wilson, C. E., de Bruijn, J. D., van Blitterswijk, C. A., Verbout, A. J. & Dhert, W. J. Design and fabrication of standardized hydroxyapatite scaffolds with a defined macro-architecture by rapid prototyping for bone-tissue-engineering research. *J. Biomed. Mate.r Res. A* **68,** 123–132 (2004).

46. Zein, I., Hutmacher, D. W., Tan, K. C. & Teoh, S. H. Fused deposition modeling of novel scaffold architectures for tissue engineering applications. *Biomaterials* **23,** 1169–1185 (2002).

47. Koegler, W. S. & Griffith, L. G. Osteoblast response to PLGA tissue engineering scaffolds with PEO modified surface chemistries and demonstration of patterned cell response. *Biomaterials* **25,** 2819–2830 (2004).

48. Taboas, J. M., Maddox, R. D., Krebsbach, P. H. & Hollister, S. J. Indirect solid free form fabrication of local and global porous, biomimetic and composite 3D polymer-ceramic scaffolds. *Biomaterials* **24,** 181–194 (2003).

49. Park, A., Wu, B. & Griffith, L. G. Integration of surface modification and 3D fabrication techniques to prepare patterned poly(L-lactide) substrates allowing regionally selective cell adhesion. *J. Biomater. Sci. Polym. Edn* **9,** 89–110 (1998).

50. Goulet, R. W. *et al.* The relationship between the structural and orthogonal compressive properties of trabecular bone, *J. Biomech.* **27m** 375–389 (1994).

51. Hayashi, K. in *Biomechanics of soft tissue in cardiovascular systems* (eds Holzapfel, G. & Ogden, R. W.) 15–64 (Springer, New York, 2003).

52. Ma, P. X. & Choi, J. W. Biodegradable polymer scaffolds with well-defined interconnected spherical pore network. *Tissue Eng.* **7,** 23–33 (2001).

53. Murphy, W. L., Dennis, R. G., Kileny, J. L. & Mooney, D. J. Salt fusion: an approach to improve pore interconnectivity within tissue engineering scaffolds. *Tissue Eng.* **8,** 43–52 (2002).

54. Sherwood, J. K. *et al.* A three-dimensional osteochondral composite scaffold for articular cartilage repair. *Biomaterials* **23,** 4739–4751 (2002).

55. Hutmacher, D. W. *et al.* Mechanical properties and cell cultural response of polycaprolactone scaffolds designed and fabricated via fused deposition modeling. *J. Biomed. Mater. Res.* **55,** 203–216 (2001).

56. Williams, J. L. *et al.* Bone tissue engineering using polycaprolactone scaffolds fabricated via selective laser sintering. *Biomaterials* **26,** 4817–4827 (2005).

57. Chu, T. M., Orton, D. G., Hollister, S. J., Feinberg, S. E. & Halloran, J. W. Mechanical and in vivo performance of hydroxyapatite implants with controlled architectures. *Biomaterials* **23,** 1283–1293 (2002).

58. Woodfield, T. B. *et al.* Design of porous scaffolds for cartilage tissue engineering using a three-dimensional fiber-deposition technique. *Biomaterials* **25,** 4149–4161 (2004).

59. Malda, J. *et al.* The effect of PEGT/PBT scaffold architecture on oxygen gradients in tissue engineered cartilaginous constructs. *Biomaterials* **25,** 5773–5780 (2004).

60. Malda, J. *et al.* The effect of PEGT/PBT scaffold architecture on the composition of tissue engineered cartilage. *Biomaterials* **26,** 63–72 (2005).

61. Saito, E., Partee, B., Das, S. & Hollister, S. J. Engineered wavy fibered polycaprolactone soft tissue scaffolds: design, fabrication and mechanical testing. *Trans. 51st Orthopaedic Research Society Meeting* **51,** 1794 (2005).

62. Fisher, J. P. *et al.* Soft and hard tissue response to photocrosslinked poly(propylene fumarate) scaffolds in a rabbit model. *J. Biomed. Mater. Res.* **59,** 547–556 (2002).

63. Rohner, D., Hutmacher, D. W., Cheng, T. K., Oberholzer, M. & Hammer, B. In vivo efficacy of bone marrow-coated polycaprolactone scaffolds for the reconstruction of orbital defects in the pig. *J. Biomed. Mater. Res.* **66B,** 574–580 (2003).

64. Roy, T. D. *et al.* Performance of degradable composite bone repair products made via three-dimensional fabrication techniques. *J. Biomed. Mater. Res.* **66A,** 283–291 (2003).

65. Simon, J. L. *et al.* Engineered cellular response to scaffold architecture in a rabbit trephine defect. *J. Biomed. Mater. Res.* **66A,** 275–282 (2003).

66. Hollister, S. J. *et al.* Engineering craniofacial scaffolds. *Orthod. Craniofac. Res.* (in the press).

67. Lin, C. Y. *et al.* Functional bone tissue engineering using ex vivo gene therapy and topology optimized, biodegradable polymer composite scaffolds. *Tissue Eng.* (in the press).

68. Schek, R. M., Taboas, J.M., Segvich, S.J., Hollister, S. J. & Krebsbach, P. H. Engineered osteochondral grafts using biphasic composite solid free-form fabricated scaffolds. *Tissue Eng.* **10,** 1376–1385 (2004).

69. Wilson, W. C. Jr & Boland, T. Cell and organ printing 1: protein and cell printers. *Anat. Rec.* **272A,** 491–496 (2003).

70. Roth, E. A. *et al.* Inkjet printing for high throughput cell patterning. *Biomaterials* **25,** 3707–3715 (2004).

71. Xu, T., Jin, J., Gregory, C., Hickman, J. J. & Boland, T. Inkjet printing of viable mammalian cells. *Biomaterials* **26,** 93–99 (2005).

72. Hollister, S. J. & Bergman, T. L. in *Additive/Subtractive Manufacturing Research and Development in Europe* (WTEC, www.wtec.org) (in the press).

73. Cohen, D. L., Maher, S., Rawlinson, J., Lipson, H. & Bonassar, L. J. Direct freeform fabrication of living cell-seeded alginate hydrogel implants in anatomic shapes. *Trans. Orthopaedic Res. Soc.* **51,** 1781 (2005).

74. Friedman, J. A. *et al.* Biodegradable polymer grafts for surgical repair of the injured spinal cord. *Neurosurgery* **51,** 742–751 (2002).

## Competing financial interests

The author declares no competing financial interests.

# ERRATUM

## Porous scaffold design for tissue engineering

SCOTT J. HOLLISTER

In this Progress Article, the caption for Figure 6 was incorrect; the correct wording is below.

**Figure 6** Cartilage regeneration by chondrocyte delivery on designed Bioplotter-fabricated PEG/PBT scaffolds is superior to PEG/PBT scaffolds made by porogen leaching. **a**, PEG/PBT scaffold fabricated by porogen leaching. **b**, Bioplotter-fabricated PEG/PBT scaffold. **c**, Cartilage matrix (red areas) generation in Bioplotter scaffold after 21 days in a mouse. Insert shows scaffold implanted without chondrocytes. **d**, Cartilage matrix (red area) generation after 21 days in scaffold made by porogen leaching. Insert shows control scaffold implanted without chondrocytes. Reprinted from ref. 60. Copyright (2005), with permission from Elsevier.